

## CERES: A SET OF AUTOMATED ROUTINES FOR ECHELLE SPECTRA

RAFAEL BRAHM<sup>1,2,3</sup>, ANDRÉS JORDÁN<sup>1,2</sup>, NÉSTOR ESPINOZA<sup>1,2</sup>

*Draft version 3 December 19, 2016*

### ABSTRACT

We present the Collection of Elemental Routines for Echelle Spectra (CERES). These routines were developed for the construction of automated pipelines for the reduction, extraction and analysis of spectra acquired with different instruments, allowing the obtention of homogeneous and standardised results. This modular code includes tools for handling the different steps of the processing: CCD image reductions, identification and tracing of the echelle orders, optimal and rectangular extraction, computation of the wavelength solution, estimation of radial velocities, and rough and fast estimation of the atmospheric parameters. Currently, CERES has been used to develop automated pipelines for thirteen different spectrographs, namely CORALIE, FEROS, HARPS, ESPaDOnS, FIES, PUCHEROS, FIDEOS, CAFE, DuPont/Echelle, Magellan/Mike, Keck/HIRES, Magellan/PFS and APO/ARCES, but the routines can be easily used in order to deal with data coming from other spectrographs. We show the high precision in radial velocity that CERES achieves for some of these instruments and we briefly summarize some results that have already been obtained using the CERES pipelines.

*Keywords:* spectroscopy

### 1. INTRODUCTION

The possibility of obtaining at the same time high spectral resolution and wide spectral coverage has made echelle spectrographs a highly demanded type of instrument. Nowadays, most astronomical facilities count with at least one of these spectrographs (see e.g. Vogt et al., 1994; Dekker et al., 2000; Noguchi et al., 2002) and they are vastly used for a wide list of astronomical applications, like the study stellar atmospheres and the search of stellar and substellar companions by measuring radial velocity variations. In particular, the development of echelle spectrographs has significantly raised in the last couple of decades due to the high radial velocity precision that they can achieve with careful calibration, a capability that has been used for discovering  $\approx 500$  extrasolar planets (e.g. Mayor & Queloz, 1995; Giguere et al., 2015).

One of the drawbacks of echelle spectrographs compared to typical spectrographs is the relative complexity demanded in the data reduction process, due to the fact that it contains several instrumental artefacts that need to be removed in order to extract a wavelength calibrated spectrum amenable for astrophysical analysis. The major complexity relies in the presence of multiple orders. These orders have quite different intensity levels due to wavelength dependent efficiency of the instrument which can obstruct their identification in some cases. Additionally, these orders have in general a significant curvature which has to be taken into account during the extraction and in some particular cases contiguous orders tend to overlap each other in the vertical direction which difficults a proper estimation of the scattered light. Moreover, echelle spectrographs can contain

additional calibration fibres and image slicers that further complicate the processing of the data. An important fraction of current echelle spectrographs have their own reduction pipelines specifically designed for the properties of each instrument (e.g. Bochanski et al., 2009; Mink, 2011), while in other particular cases there is no dedicated pipeline at all. This fact can produce some inconsistencies when spectra obtained from different instruments are used in the same analysis, in particular when the reduction steps include human intervention. Even in the case of working with data of a particular telescope, the automatization of the data processing is desirable and is specially crucial when working on obtaining precision radial velocities at different epochs, because slight changes in the reduction steps can introduce significant systematic effects that propagate to the estimation of the Doppler shifts.

There have been already some attempts to develop computational tools for the automated processing of data originated from different echelle spectrographs, but their use has not been extended for more than a couple of instruments so far. For example, Mills et al. (2003) presented the open source code ECHOMOP, which has been mostly used in the processing of data obtained from the Utrecht Echelle Spectrograph of the 4.2-m William Hershell Telescope, while Sosnowska et al. (2015) presented the flexible reduction library for the ESPRESSO project which is also able to process data from HARPS and HARPS-N. Along the same line, the MIDAS system (Banse et al., 1983) developed by ESO included a package designed to process echelle spectra (Ballester, 1992), which has been used to develop pipelines for most of ESO spectrographs.

In this paper we present a new set of computational routines for developing fully automated reduction pipelines for data of echelle spectrographs. This modular code called CERES (Collection of Elemental Routines for Echelle Spectra) is mostly written in Python, but contains also C and Fortran routines when speedy execu-

<sup>1</sup> Instituto de Astrofísica, Facultad de Física, Pontificia Universidad Católica de Chile, Av. Vicuña Mackenna 4860, 782-0436 Macul, Santiago, Chile

<sup>2</sup> Millennium Institute of Astrophysics, Av. Vicuña Mackenna 4860, 782-0436 Macul, Santiago, Chile

<sup>3</sup> rbrahm@astro.puc.cl, the CERES code can be downloaded from <https://github.com/rabrahm/ceres>

tion demands it. We have developed reduction pipelines for thirteen different spectrographs, and these recipes can be used as a guide for building pipelines for other instruments. The principal aim of the pipelines that we have developed is the handling of low signal to noise ratio data and the measurement of precision radial velocities in the context of extrasolar planets.

In § 2 we describe the structure of the CERES echelle pipelines and the corresponding variations for each type of spectrograph. In § 3 we list the instruments that are currently supported by CERES, while in § 4 we discuss the performance of some of the CERES pipelines. Finally, in § 5 we summarise our work.

## 2. STRUCTURE AND REDUCTION STEPS

### 2.1. General considerations

The main purpose of the CERES routines is the development of completely automated pipelines that are able to generate optimally extracted, wavelength calibrated and instrumentally corrected spectra, plus additional parameters like radial velocities, bisector spans and stellar atmospheric parameters. The input is raw images of echelle spectrographs, and we aim to fully avoid the need for human intervention in the process. CERES routines have been successfully implemented for handling data of echelle spectrographs with quite different specifications, including fibre-fed and slit spectrographs. A description of the particular functions used by CERES can be found in the github repository<sup>4</sup>

All CERES pipelines have the same general structure. They have a main code that drives all the steps required to obtain a reduced and analysed spectrum. The main code can call functions from a general module that contains tasks that can be used by different pipelines (GLOBALutils), but it can also call functions from another Python module that contains tasks specifically designed for a particular instrument. In this way, the different CERES pipelines mostly use the same functions in which the parameters change according to the instrument specifications. However, there are some specific functions for which the operations can be structurally different. Most of the tools are coded in Python but there are also some time-consuming tasks for which we wrote code in C but which are wrapped to be called directly from Python. Some of the time consuming tasks have been also parallelized to further accelerate the reduction process. Even though all pipelines share a similar structure, there are several particular differences due to the differing properties of each instrument.

In order to simplify the description of the CERES routines we will briefly explain the structure of a typical echelle image and we will define some useful concepts. The high resolving power obtained with echelle spectrographs is achieved thanks to the high incidence angle used between the incident light and the plane grating. In other words, echelle spectrographs work at very high spectral orders. However, this configuration of the instrument produces that, after the beam is dispersed by the grating, different orders of the spectrum overlap with each other. In order to correct for this effect, a second dispersion element is used which disperses the light in

the perpendicular direction with respect to the grating and in this way separates the spectral orders. This operation allows also to fit the complete spectrum in a single rectangular CCD, which will register a set of traces corresponding to the different echelle orders. For the rest of the paper we will refer to the direction in which the beam is dispersed by the plane grating as the *dispersion direction*, while the direction in which the orders are separated with the second dispersion element will be called *cross-dispersion direction*. Moreover, for simplicity we will arbitrarily consider that the dispersion direction (cross-dispersion direction) goes in the horizontal (vertical) direction of the CCD or along its rows (columns).

### 2.2. Pre-processing

#### 2.2.1. Classification of frames

The first step of any CERES pipeline is to identify all the images that are going to be used in the reduction process and to classify them according to their types. CERES receives as input the path to the directory containing all the raw images. Given that there is no unified header keywords, a particular function has to be defined for each spectrograph that performs the classification. Common image types are: bias frames, dark frames, flat frames, wavelength calibration frames and science images. CERES reads the header of each image and according to the corresponding keywords of each instrument, proceeds to classify the images by creating lists for the different data types that contain the full names of the corresponding raw images.

#### 2.2.2. Master CCD Frames

Once the classification of the images is done, the next step is to construct the master CCD calibration images by median combination. The exact type of required calibration images strongly depends on the specifications of each instrument. Bias and dark master frames are usually not included as standard calibrations for several spectrographs but these master frames are generated if required. In the case of master dark frames, if there is no dark that matches the exposure time of a particular science image, the CERES routines interpolate the intensity of the master dark frames in order to generate one with the required exposure time. The correction of the science images is performed by subtracting the master bias frame and the corresponding master dark frame.

Flat-field correction is a relatively complex procedure in the case of echelle spectrographs. This procedure is required to correct for sensitivity variations of the detector pixels. The use of a classical flat-field in which the full detector is illuminated by an homogeneous source is not reliable in spectroscopy because the sensitivity of each pixel depends also on the particular wavelength that it receives. For this reason, the light of the source used for the flat-field correction must be also dispersed by the instrument. In the case of fibre-fed echelle spectrographs, it is physically impossible to illuminate the full detector. However, in the case of slit spectrographs, a common procedure is to obtain the spectrum of a continuum source but using a longer slit than the one used for obtaining the science spectra. Spectrographs like Magellan/MIKE (Bernstein et al., 2003) and Keck/HIRES (Vogt et al.,

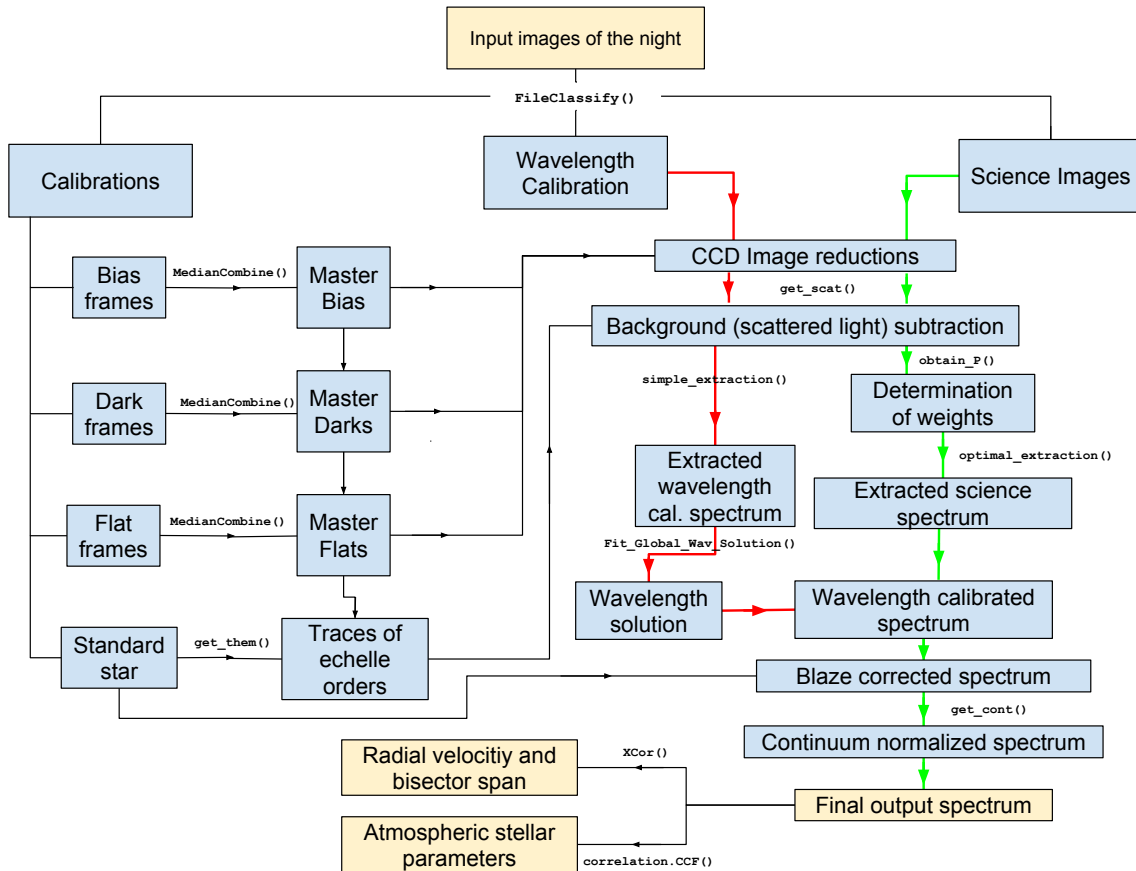


**Figure 1.** Flow diagram showing the images and processes that are in general used by the CERES pipelines for slit spectrographs. The most important functions at each step are also shown.

1994) follow this calibration procedure which ensures that the sensitivity variations of the CCD in the borderline regions of the echelle orders of the science spectra are properly corrected. We will name these type of calibration image “long-slit flat frames” from now on. What CERES actually does with long-slit flats is first to co-add them in order to generate a master long-slit flat frame. Then, after having identified and traced the echelle orders (see § 2.2.3), CERES selects the slices of this master flat that contain the echelle orders, and a 2D median filter is computed for each slice. Finally, each of the slices containing the echelle orders is divided by its corresponding median filtered surface and at the same time the inter-order regions of the image are filled with values equal to one. This normalised long-slit flat frame will contain the high frequency pixel sensitivity of the CCD with its corresponding wavelength dependence. After subtracting the bias and dark frames, the science images will be corrected by dividing them by the normalised long-slit flat frame. This procedure only corrects for the high frequency pixel variations. Some other slit spectrographs use a different approach for performing the flat-field correction. For example, for the echelle at the DuPont telescope a diffuser is placed in front of the spectrograph which spreads the dispersed light of the afternoon sky and generates a smooth and homogeneously illuminated image which conserves also the approximate wavelength dependence at each pixel. This type of image is known as miky-flat. In this case, CERES co-adds the miky-flat images in order to generate a master milky flat and then a

2D median-filtered frame is obtained of the whole image. Finally, the master milky-flat is divided by the median-filtered frame to generate the normalised milky-flat, for which the inter order regions are not modified because in this case they contain real signal. The science frames are then corrected by dividing them by the normalised milky-flat after the master bias and dark subtraction.

In the case of fibre-fed spectrographs, the flat-field correction is not attempted, which is due mostly due to the complexity of illuminating with high intensity the border regions of each echelle order. Pixel sensitivity variations for fibre-fed spectrographs are only partially corrected following another approach which is explained in § 2.5. This procedure requires images in which the spectrum of a continuum lamp is registered. This images will be called “fibre-flat frames” hereon. CERES co-adds all the fibre-flats to generate the master fibre-flat, which is then used to identify and trace the orders (see § 2.2.3), compute the weights for the optimal extraction (see § 2.5), and correct for the blaze function (see § 2.2.3).

### 2.2.3. Identification of the echelle orders

One key step in the processing of echelle data is the identification and tracing of the echelle orders. In the case of fibre-fed spectrographs, an image of the spectra of a continuum lamp is used to perform this procedure, while a spectrum of a bright object is usually used for slit spectrographs. In order to find the orders, the central columns of the image are used because usually they have higher SNR than the other zones. The exact number

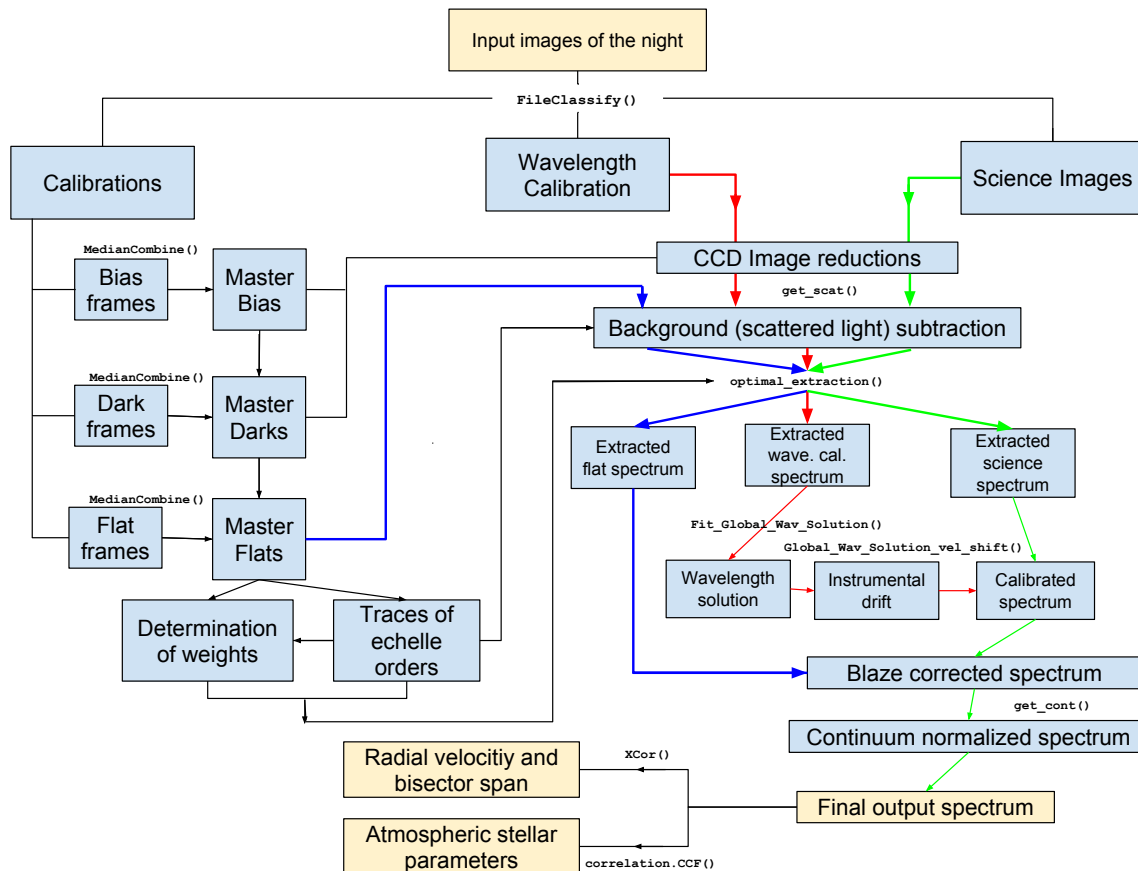


**Figure 2.** Flow diagram showing the images and processes that are in general used by the CERES pipelines for fibre-fed spectrographs. The most important functions at each step are also shown.

of columns is a free parameter that can be modified by the user but usually is of the order of 10 pixels. These columns are median combined along the dispersion direction for constructing a reference vertical cut of the CCD without cosmic rays or cosmetic artefacts. Then, this reference column is convolved with a Gaussian kernel for smoothing it, where the width of the Gaussian is another parameter that can be modified by the user. All the peaks of the smoothed reference column are identified and then an iterative procedure is applied to reject shallow peaks that have smaller counts than  $N$  times the dispersion of the counts in the inter-order zones, where  $N$  is another adjustable parameter. The left panel of Figure 3 shows the vertical cut in an image obtained with the echelle spectrograph mounted on the DuPont telescope that is used to identify the orders.

As opposed to common spectrographs, the traces of most echelle spectrographs have a strong curvature on the CCD. Starting from the central position of each order computed in the last step, the vertical position of the order in each column is identified by fitting a Gaussian in zones centered on the positions contiguous to the already identified order centers. The width of the zone where the Gaussian is fit must be similar to the approximate cross-dispersion (vertical) extension of the orders. In order to avoid errors in the tracing of the orders arising from low signal to noise, cosmic rays, or instrumental artifacts, a procedure is applied in which the drift of the orders between the new column and the previous column is computed and positions that show drifts 3 times greater than

the dispersion of the already computed drifts for that order are rejected and the centroid for those positions are replaced by the one of the contiguous position plus the median drift.

Finally a high order polynomial is fitted to the centroids computed for each order and the coefficients of the fit are saved for extracting the science and calibration spectra. The right panel of Figure 3 shows a portion of a DuPont image and the traces identified by the CERES algorithm.

Some slit spectrographs mounted directly on the telescope can suffer from strong flexures, which produce as a result that the vertical position of the orders can significantly change depending on the pointing position of the telescope. To handle this effect, CERES includes a function to retrace the orders by using the reference traces and performing a cross-correlation against the science images in pixel space. The pixel displacement of the maximum of the cross-correlation function is taken as the instrumental drift and all the reference traces are displaced by that amount.

#### 2.2.4. Scattered light subtraction

In echelle spectrographs, in addition to the dispersed light registered in each order, some scattered light generated by the echelle grating and the roughness of the optical surfaces is also detected by the CCD. This contamination produces a smooth background that has to be removed before extracting the spectra in order to conserve the true depth of the absorption lines. CERES uses

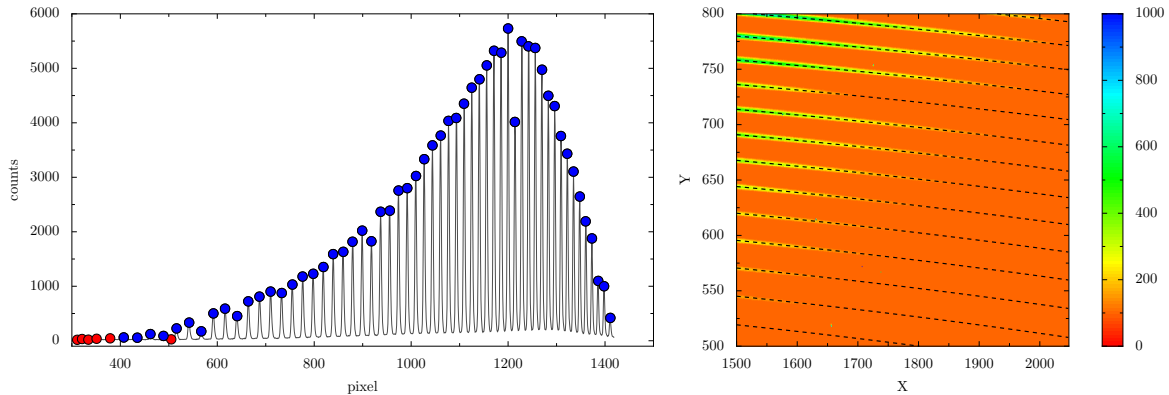


**Figure 3.** Left: vertical cut of an image of the DuPont/Echelle. The blue circles correspond to the orders identified by our algorithm while the red circles are the other maxima that are rejected. Right: portion of an echelle image used to determine the traces of the echelle orders which are displayed as dashed lines. Given that the algorithm uses the information of the complete image to trace each order, good performance is achieved even in region with low signal-to-noise ratio.

a simple algorithm to correct for this effect (`get_scat`). At this stage, the traces of the orders and their widths are already known, and this can be used to select only the inter-order zones of the image. For each column, the algorithm computes the median flux in each inter order region and then a linear interpolation of these values in the vertical (cross-dispersion) direction is performed to infer the scattered light level in the intra-order regions of the image. After performing this process for each column we will end up with a two dimensional map of the scattered light. In order to smooth the effects of spurious signals, a two dimensional median filter is applied to the constructed scattered light surface, and finally the filtered image is subtracted from each original science image.

### 2.3. Extraction

The extraction of a spectrum refers to the process of adding up all the signal around the trace in the direction perpendicular to the dispersion, going thus from a 2D image to a 1D spectrum. In the case of an echelle spectrograph the extraction process produces a 1D spectrum for each order. Before adding up the signal, all the systematic effects must be removed, which means that the master calibration frames must be applied to the science image, bad columns must be corrected and the scattered light background must be subtracted as described above.

CERES contains two algorithms for performing the extraction. The simpler one corresponds to the simple sum of the flux of all the pixels contained in a vertical window of width defined by the user. This algorithm is known as “rectangular extraction”. The second algorithm that CERES implements is called optimal extraction (Horne, 1986), which is particularly useful to obtain high quality spectra from low SNR data. This algorithm relies on the determination of the appropriate weights across the profile of the objects that produce the minimum expected variance for the expected value of the total flux, while keeping the estimator of the flux unbiased. If we denote these weights by  $W_{x,\lambda}$ , where  $x$  is the  $x$ th pixel in the direction perpendicular to the dispersion direction and  $\lambda$  is the  $\lambda$ th pixel in the dispersion direction, then the optimal extracted flux can be written as

$$F_\lambda = \sum_{x_1}^{x_2} W_{x,\lambda} F_{x,\lambda},$$

where  $F_{x,\lambda}$  is the measured flux in the CCD in the  $x$ th and  $\lambda$ th pixel, and  $x_1$  and  $x_2$  are the limits of the vertical window whose width is defined by the user (note that, for rectangular extraction,  $W_{x,\lambda} = 1$ ). The idea of Horne (1986) is to express these weights in terms of the fraction of the flux of the object in the  $x$  direction,  $P_{x,\lambda} = F_{x,\lambda} / \sum_{x'=x_1}^{x'=x_2} F_{x',\lambda}$  (note that this constrain implies that  $\sum_{x=x_1}^{x=x_2} P_{x,\lambda} = 1$ ). By imposing the minimum variance and unbiasedness conditions on the retrieved flux, it is easy to show that

$$W_{x,\lambda} = \frac{P_{x,\lambda} / \text{Var}(F_{x,\lambda})}{\sum_{x_1}^{x_2} P_{x,\lambda}^2 / \text{Var}(F_{x,\lambda})},$$

where  $\text{Var}(F_{x,\lambda})$  is the variance of the flux in the  $x$ th and  $\lambda$ th pixel which in this model is given by  $F_\lambda P_{x,\lambda} / G + \text{RON} / G^2$ , where  $G$  is the detector gain and RON is the readout noise. In order to obtain the weights, the original algorithm of Horne (1986) assumes the  $P_{x,\lambda}$  are smooth functions in  $\lambda$  and, thus, modelled them as low order polynomials in  $\lambda$  subject to being normalized in the  $x$  direction (i.e.,  $\sum_{x=x_1}^{x=x_2} P_{x,\lambda} = 1$ ). However, echelle spectra are typically highly distorted in the  $x$  direction as well. We thus follow Marsh (1989) who extends this idea to deal with highly distorted spectra by modelling the  $P_{x,\lambda}$  not in the  $x$  direction, but in the actual traces of the spectra. The strategy deals with the problem by fitting  $K$  different polynomials positioned parallel to each other along the traces and separated by a distance  $S$ .

The number of polynomials,  $K$ , must be higher than the width in pixels of the order and can be modified by the user. The distance  $S$  is automatically calculated using the width in pixels and this number of polynomials. The polynomials are computed in an iterative process which allows to identify cosmic rays and correct for them. In the case of stable fibre-fed spectrographs, the weights are computed from a calibration image known as a fibre flat, which corresponds to a spectrum of a continuum lamp. In the case of slit spectrographs, the weights are computed from the same science images that are being extracted.

## 2.4. Wavelength Calibration

### 2.4.1. ThAr lamps

The most common procedure for calibrating the science spectra in wavelength is to use the spectrum of a reference lamp filled with a particular gas. When this gas is heated it radiates only in certain narrow emission lines according to the particular allowed electronic transitions of the atoms present in the gas. If the lamp has been characterized, it can be used to generate a mapping between the pixel position and the corresponding wavelength. This type of light source is commonly known as arc lamp, and depending on the particular wavelength range of interest, the arc lamp can contain different combination of gases (H, He, Ne, Ar, Na, Cu, Hg). In the case of high resolution optical echelle spectrographs the most commonly used calibration lamp nowadays is one composed of Thorium (Th) and Argon (Ar).

The extraction procedure adopted for the spectra of the ThAr lamps depends on the type of spectrograph used. For fibre-feb spectrographs the extraction is performed exactly as it is performed for stellar spectra, which means that the weights determined from the flat frames are used by the optimal extraction algorithm. In the case of slit spectrographs, due to the absence of a reference profile for determining the weights, the simpler rectangular extraction method is used.

Once the spectra of the ThAr lamp have been extracted, the process to compute the wavelength solution is the same one for every spectrograph. Nonetheless, for each spectrograph a specific reference line list is required. The exact format of this set of reference lines is as follows. For each echelle order, the pipeline requires the existence of a text file in the *wavcals* directory which is located inside the directory containing the particular pipeline. These files must contain at least two columns, the first one containing the approximate pixel position of the ThAr lines present in the corresponding echelle order ( $x_i^{ap}$ ), while the second column should contain the associated wavelength value of the emission line ( $\lambda_i$ ).

Given that for some spectrographs the pixel position of the emission lines can drift significantly on a timescale on the order of days, months or years, the pipeline first computes a rough estimation of this long-term instrumental drift in the dispersion direction measured in pixels ( $\Delta_p$ ).  $\Delta_p$  is obtained by computing the order-by-order cross-correlation function between the corresponding extracted ThAr spectrum and a binary mask. This binary mask is constructed from the reference text files, where it takes values equal to one in the regions containing emission lines, and values equal to zero elsewhere. The cross-correlation functions for all the orders are combined, and the position of the maximum of the summed cross-correlation function is assumed as  $\Delta_p$ , which is then applied to shift the approximate pixel positions of all the emission lines defined in the reference text files. For stabilised spectrographs like HARPS, FEROS, or Coralie, this procedure is not strictly required because their long-term instrumental drifts are smaller than one pixel.

The next step performed by the pipeline is to determine a more precise value of the pixel position of each emission line for the analysed ThAr spectrum. To achieve this goal, Gaussian functions are fitted to the extracted ThAr spectrum in zones around  $x_i^{ap}$ . The mean of each Gaussian is used as the precise pixel position of the emission lines  $x_i$ . After this procedure each emission line  $i$  possesses a wavelength value ( $\lambda_i$ ), a precise pixel

position ( $x_i$ ) and an echelle order ( $j_i$ ), which extends from 0 to the number of detected orders minus 1, ordered from the reddest to the bluest. In order to achieve the highest precision possible CERES routines have a careful treatment of zones with blended emission lines. These zones can be defined in the reference text file, and the algorithm will fit multiple Gaussians in those regions of the spectrum.

The next step consists in fitting iteratively a polynomial between  $\{x_i\}$  and  $\{\lambda_i\}$  for each echelle order  $j$ . In this process CERES rejects strong outliers that correspond to poorly identified emission lines. This procedure delivers also the approximate wavelength value of the central pixel of each echelle order  $j$  ( $\lambda_j^c$ ), which can be used to determine the *real* order numbers  $\{m_j\}$  of the instrument<sup>5</sup>. In practise, we search for the integer  $m_0$  such that

$$m_0 + j = m_j. \quad (1)$$

The grating equation states that  $\lambda \propto m^{-1}$  and therefore the correct  $m_0$  value will be the one that produces the smaller slope of the following equation:

$$y(j) = (m_0 + j)\lambda_j^c. \quad (2)$$

Once  $m_0$  has been determined, each emission line will have also its corresponding *real* echelle order  $m_i = j_i + m_0$ .

Once the *real* order numbers are known, the pipeline computes a global wavelength solution in the form of an expansion of the grating equation (see Section 2.6 in Baranne et al., 1996) using Chebyshev polynomials. This fit includes also a  $3\sigma$  iterative procedure in which more outlier emission lines are rejected.

In detail, our global wavelength solution takes the form

$$\lambda(x, m) = \frac{1}{m} \sum_{i=0}^{n_m} \sum_{j=0}^{n_x} a_{ij} c^i(m) c^j(x), \quad (3)$$

where  $x$  and  $m$  refer to the pixel value and echelle order number, respectively,  $c^n$  denotes the Chebyshev polynomial of order  $n$ ,  $a_{ij}$  are the coefficients that are fitted to obtain the wavelength solution,  $n_m$  is the degree of the Chebyshev polynomial in  $m$  and  $n_x$  is the degree of the Chebyshev polynomial in  $x$ . The values of  $n_m$  and  $n_x$  will depend on the particular properties of each instrument and for our set of pipelines they were determined by visually inspecting if there was any structure in the residuals of the wavelength solutions. Figure 4 shows an example of a global wavelength solution of the FEROS spectrograph. The bottom panel of that figure shows that the residuals in the wavelength position of the ThAr emission lines are in general below 0.003 Å.

The reference wavelength solution of a given night is usually obtained with the calibration frames taken in the afternoon and posterior ThAr spectra are obtained during the night to monitor any instrumental drifts of the system. In the case of unstabilised instruments like the ones mounted on the telescope or the ones that are not controlled in temperature and pressure, additional ThAr exposures must be obtained before and after each science

<sup>5</sup> By “real” order numbers we refer to the physical order that corresponds to the one appearing on the grating equation.

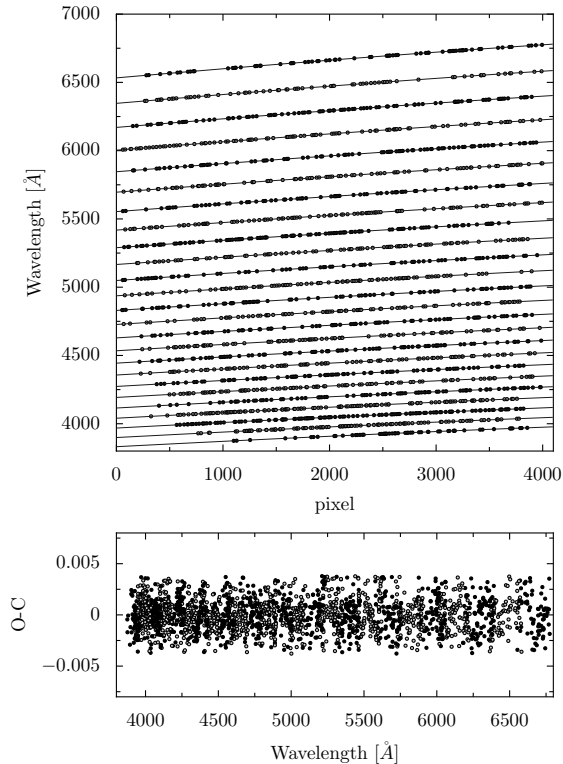


**Figure 4.** Top panel: global wavelength solution that produces the best fit to the positions of the emission lines of a ThAr lamp observed with the FEROS spectrograph. The circles correspond to the wavelength of the particular emission lines that are used in the fit. The solid line is the fitted global solution. Bottom panel: residuals produced with the global wavelength solution of the top panel.

image in order to obtain the best RV precision achievable. For stabilised instruments like HARPS, CORALIE and FEROS the acquisition of ThAr spectra during the night may be not mandatory. However, in the case of these instruments, a second fibre is always available for obtaining a simultaneous ThAr spectrum while observing the science target to trace subtle instrumental drifts.

In order to determine the velocity drift of a given ThAr spectrum with respect to the ThAr spectrum that was used to compute the reference wavelength solution, the pipeline first identifies the set of  $\{x_i\}$ ,  $\{\lambda_i\}$  and  $\{m_i\}$  values for the new ThAr spectrum following the same steps described in the previous paragraphs. However, then, instead of searching for new Chebyshev coefficients by fitting equation 3, the pipeline assumes that the wavelength solution should have been modified just by a multiplicative Doppler factor, and therefore the  $a_{ij}$  coefficients of the reference wavelength solution are held fixed and the set of  $\{x_i\}$ ,  $\{\lambda_i\}$  and  $\{m_i\}$  values are fitted to the following model:

$$\lambda(x, m) = \frac{1}{m} \left( 1 + \frac{\delta v_{inst}}{c} \right) \sum_{i=0}^{n_m} \sum_{j=0}^{n_x} a_{ij} c^i(m) c^j(x), \quad (4)$$

which contains only a single free parameter  $\delta v_{inst}$  that corresponds to the velocity Doppler shift between both ThAr spectra.

#### 2.4.2. Fabry-Perot system

Even though the use of ThAr lamps allows to achieve very precise wavelength solutions that enable the computation of precise RVs, they are quite far from being perfect calibrators. Only few emission lines are generally visible in the bluer ( $\lambda < 4000 \text{ \AA}$ ) and redder ( $\lambda > 7000 \text{ \AA}$ ) parts of the wavelength coverage. The intensities of the lines are not uniform, which produces the saturation of some lines in some orders in order to allow the detection of fainter ones. In some cases when the simultaneous calibration lamp is used, the saturation of some ThAr lines can even contaminate contiguous orders dedicated to obtain the science spectra. Moreover, the internal composition of the lamps can change, which can produce long term instrumental drifts in the measured RVs. Also, they do expire at some point and some subtle manufacturing differences in the lamps can induce other systematic errors when a new lamp is installed. A couple of alternative wavelength calibration systems have been developed with the goal of replacing the use of the ThAr lamps. The most promising one is the laser frequency comb (Li et al., 2008), which produces a forest of emission lines with similar intensities whose exact wavelength positions can be synchronized with radio-frequency oscillators referenced to atomic clocks. However, the cost of such systems is rather high and they are still under study and development. An alternative approach is the use of Fabry-Perot interferometers (Halverson et al., 2014; Reinert et al., 2014; Sarmiento et al., 2014; Stürmer et al., 2016), in which a pair of parallel reflecting surfaces that are illuminated with a continuum source produce a fringed pattern due to the constructive and destructive interference that arises from the interaction of the light reflected in both surfaces. The spectra produced by a Fabry-Perot system are populated with a forest of emission lines that extend across the full wavelength coverage of the spectrograph and where the separation between two contiguous lines depends on the effective distance of the two reflective plates. With this type of systems, the long term precision of the wavelength calibration does not depend on the source lamp and only on the properties of the reflective plates.

One of the major drawbacks of Fabry-Perot interferometers as wavelength calibration systems is that they do not deliver directly an absolute wavelength calibration as opposed to ThAr lamps where the characteristic pattern of the spectrum can be used to associate specific wavelengths to each line. What is commonly done in spectrographs like CORALIE is to compute the absolute wavelength calibration with the spectrum of a ThAr lamp obtained in the afternoon calibrations. Immediately after that, the absolute solution is then improved with the acquirement of Fabry-Perot spectra. The instrumental drifts during the night are calculated then by the acquirement of Fabry-Perot spectra with the comparison fibre. With this procedure the ThAr lamp is only marginally used, extending its useful life, the wavelength solution is determined with higher accuracy and the science observations do not suffer from the contamination of saturated ThAr lines.

CERES includes the functions required for handling Fabry-Perot calibration spectra and they have been added to the pipeline that handles data from the CORALIE spectrograph. In this case, for computing the wavelength

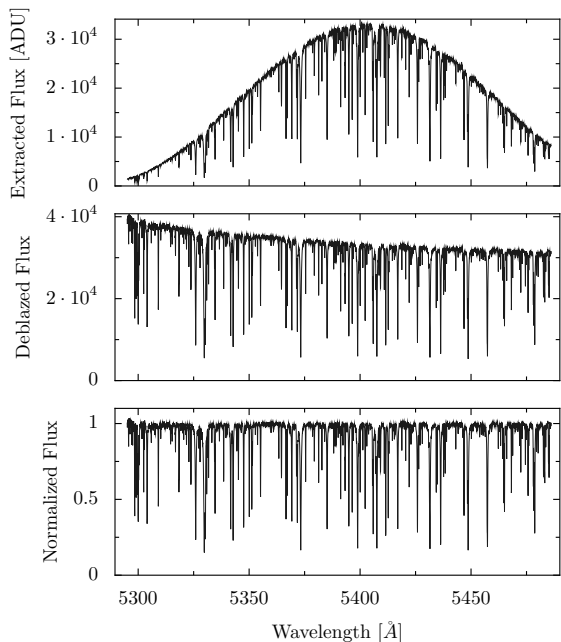


**Figure 5.** Top panel: Optimally extracted FEROS spectrum of the star HD72673 for a particular echelle order. Central panel: Extracted spectrum divided by the blaze function, which is obtained for the flat frames in this case. Bottom panel: continuum normalised spectrum obtained with by a polynomial fitting of the debased spectrum.

calibration of a science spectrum, 3 images are required: the ThAr lamp at both fibres (TH2), the ThAr lamp at the object fibre while the Fabry-Perot is at the comparison fibre (THFP); and the stellar spectra at the object fibre while the Fabry-Perot is at the comparison fibre (OBFP). The global absolute wavelength solution is computed for both fibres with the reduced spectra of TH2. Then, the Fabry-Perot spectra of the comparison fibre in THFP is calibrated in wavelength by the computation of  $\delta v_{inst}^1$  between the ThAr spectra of the TH2 and THFP images using equation 4. Finally the instrumental drift  $\delta v_{inst}^2$  between the THFP and the OBFP images is calculated via the computation of the cross-correlation function between both Fabry-Perot spectra.

## 2.5. Final output and post-processing

### 2.6. Final output

Several outputs are produced after each pipeline is executed. The reduced spectrum is saved in a three dimensional fits file with the following general form: [data type,echelle order,pixel]. The data type dimension has generally eight entries. The first entry ([0, :, :]) is the matrix containing the wavelengths of each pixel for each echelle order after computing all the instrumental velocity drifts. The second entry ([1, :, :]) corresponds to the optimally extracted stellar flux. The top panel of Figure 5 shows the extracted flux of a G-type star for one order obtained with the FEROS spectrograph. The third entry contains a measure of the error associated to the extracted flux (Inverse variance).

The fourth entry corresponds to the deblazed stellar flux (central panel of Figure 5) and the fifth entry contains its associated inverse variance. In echelle spectrographs, the flux of each order registered by the CCD contains a strong instrumental modulation which has to

be corrected in order to be analysed. This instrumental effect is known as the blaze function and it is produced due to interferences in the echelle grating, and therefore it depends on its blaze angle. There are several approaches that can be followed to correct for the blaze function. The complexity of the chosen method depends on the purpose that the science spectra will have. Given that the main purpose of the CERES pipelines is the use of the narrow stellar absorption lines for computing precision radial velocities and the determination of stellar atmospheric parameters, the large scale modulations of the spectrum do not present a fundamental problem. For this reason, CERES uses simple procedures for estimating the blaze function.

In the case of fibre-fed spectrographs, the blaze function of the science spectra is partially corrected by using the *fibre flat frames* described in § 2.2.2. After correcting for scattered-light, the master fibre flat frame is extracted following the same procedure used for the science spectra, and then each extracted order of the flat frame is normalised by its maximum. This normalised flat spectrum is assumed to represent an approximation of the blaze function. The correction for the blaze function of the science spectra is performed by dividing the extracted spectrum of each order by the corresponding normalised flat spectrum. This procedure also corrects for the column-averaged pixel-to-pixel variations of the CCD.

For echelle spectrographs using slits, CERES estimates the blaze function by using the spectrum of a hot and rapidly rotating star where a high order polynomial is fitted to the spectrum of each echelle order.

However, for both type of spectrographs, given the differences in the continuum emission of the observed star and the blaze correcting object (flat lamp or rapidly rotating star), the deblazed spectra will end up having a particular slope or smooth variation that will not reflect the shape of the continuum of the observed star. The recovery of the stellar continuum can be only found if the spectral energy distribution of the calibrator is accurately known, and flux calibration of echelle spectrographs is notoriously difficult (e.g. Suzuki et al., 2003). However, as was already explained, the main goal of the CERES pipelines is to use of the narrow absorption lines, and therefore the exact shape of the stellar continuum is not required. For this reason the sixth and seventh entries of the output of the CERES pipelines correspond to the continuum normalized flux and its associated inverse variance, respectively (bottom panel of Figure 5). The continuum normalisation is obtained by fitting a low order polynomial to the deblazed flux including an iterative procedure that excludes absorption lines from the fit. Finally the eighth column corresponds to the SNR per pixel in the continuum of the observed spectrum. The SNR is estimated by combining the contribution of (i) the expected Poisson error at each pixel given the extracted flux, (ii) the read out noise, and (iii) the expected Poisson error at each pixel produced by the scattered light.

In addition to the reduced and wavelength calibrated spectra CERES contains several functions that are used by the pipelines to analyse the spectra in an homogeneous way, as we now detail.

#### 2.6.1. Radial Velocities

The information about the velocity of the observed star is contained in the wavelength position of its spectral lines. Griffin (1967) showed that a very efficient way for using simultaneously the information provided by all the observed lines for measuring precise radial velocities is to use the cross-correlation function (CCF), which can be used even with low signal-to-noise ratio data. Following this principle, CERES includes a set of functions for the computation of the CCF using a binary mask (Baranne et al., 1996). The mask takes values equal to 1 in the regions where a typical stellar spectra contains narrow absorption lines and equal to 0 elsewhere. The exact regions of the mask associated with absorption lines will depend on the atmospheric properties of the star (principally on  $T_{\text{eff}}$ ). For this reason there are 3 available masks for 3 different spectral types (G2, K5 and M5) that can be used to compute the RV of the observed spectrum. These masks are the same ones used by the data reduction system of HARPS (Mayor et al., 2003). The default mask for all the pipelines is the G2 but it can be changed by the user if the properties of the observed star are known and are closer to the ones of the other masks. However, we note that it is key to analyse all the spectra of a particular star with the same mask, because the use of different masks will produce different zero point velocities that can be responsible of increasing the dispersion of the radial velocity measurements, hindering the detection of a Keplerian variation.

The algorithm that computes the CCF includes the effects of pixelization and computes one CCF for each echelle order before combining them using a weighted sum according to the median SNR of each order. The CCF for the echelle order  $m$  at a certain velocity  $v$  can be expressed as

$$CCF^m(v) = \frac{\int_{\lambda_i}^{\lambda_f} W(\lambda') F(\lambda) M(\lambda') d\lambda}{\sqrt{\int_{\lambda_i}^{\lambda_f} W(\lambda') M(\lambda')^2}}, \quad (5)$$

where  $\lambda_i$  and  $\lambda_f$  are the wavelengths of the initial and final pixels of the order  $m$ ,  $F(\lambda)$  corresponds to the observed spectrum,  $W(\lambda')$  corresponds to the weight that each spectral zone has according to the binary mask and  $M(\lambda')$  is the binary mask shifted to the  $\lambda' = \lambda(1 + v/c)$  wavelength positions due to the Doppler displacement, where  $c$  is the speed of light. As defined in equation 5, the CCF will acquire its minimum values for  $v$  close to the radial velocity of the observed star. The actual RV is computed by fitting a Gaussian to the CCF, and the resulting mean is taken to be the RV of the star. The left panel of Figure 6 shows an example of a CCF computed from a FEROS spectrum and its corresponding fitted Gaussian.

During nights with a bright Moon, the spectrum of the Sun reflected by the Moon can strongly contaminate the spectrum of the target star producing an additional peak in the CCF that can systematically alter the measured radial velocity of the star. Different methods for correcting for this effect have been proposed in the recent years (e.g. Cabrera et al., 2010; Halverson et al., 2016). CERES also includes tools for determining the impact that moonlight contamination produces on the radial velocities. Using the `pyephem` package we compute the coordinates that the moon possesses at the time of

the observations and we also estimate the radial velocity at which the solar spectrum should show up in the CCF. In addition, from previous simulations we also know the width of the CCF peak produced by this contaminant. If the Moon is above the horizon and produces an important peak in the CCF close to the one produced by the star, then we simultaneously fit two Gaussians to the computed CCF, where the Gaussian corresponding to reflected sunlight has only one free parameter, namely the depth of the peak produced by the moonlight contamination. The right panel of Figure 6 shows a CCF that is heavily contaminated and the corresponding best fit of Gaussians.

Uncertainties on the radial velocities are determined from the width of the CCF and the mean signal-to-noise ratio close to the Mg triplet zone using empirical scaling relations (as in Queloz, 1995) whose parameters are determined using Monte Carlo simulations. The exact equation used to estimate the RV error is

$$\sigma_{RV} = b + \frac{a(1.6 + 0.2\sigma_{ccf})}{SN_{5130}}, \quad (6)$$

where  $a$  and  $b$  are the coefficients obtained via the Monte Carlo simulations and depend on the applied mask,  $SN_{5130}$  is the continuum SNR at 5130 Å and  $\sigma_{ccf}$  is the dispersion of the Gaussian fit to the CCF.

Our Monte Carlo simulations were performed for every spectrograph that is supported by CERES. We use high SNR extracted spectra, to which artificial Gaussian noise is added. The amplitude of the noise varies along each echelle order by taking the blaze function into account. This artificial spectrum is then continuum normalised and we compute its radial velocity using equation 5. For a given noise amplitude, this process is repeated  $\sim 1000$  times and we save the standard deviation ( $\sigma_{RV}$ ) of the sample of computed radial velocities. This procedure is repeated with different noise amplitudes in order to have an estimation of  $\sigma_{RV}$  for different values SNR. In addition we use spectra with different stellar atmospheric parameters which produce different widths of the cross-correlation peak ( $\sigma_{ccf}$ ). The sets of SNR,  $\sigma_{RV}$  and  $\sigma_{ccf}$  obtained with these simulation were then fitted with the function specified in equation 6 in order to determine the appropriate  $a$  and  $b$  coefficients for each instrument. For illustration, the values of the coefficients for the G2 mask in the case of the Coralie spectrograph are  $a = 0.06544$  and  $b = 0.00146$  (in  $\text{km s}^{-1}$ ).

In order to measure the RV variations in a star produced by a planetary companion it is required to correct the RV of the observed spectra for the velocity that the observer has with respect to the star. This procedure is known as the barycentric correction and consists in computing the velocity that the observatory has with respect to the barycentre of the solar system projected in the direction of the observed star. The two principal velocities that have to be computed are the movement of the earth around the barycentre and the rotation of the earth at the geographical coordinates of the observatory. In order to determine the barycentric correction CERES uses the `jplephem`<sup>6</sup> python client of the Jet Propulsion Laboratory ephemerides package which is written mostly in

<sup>6</sup> [http://www.cv.nrao.edu/~rfisher/Python/py\\_solar\\_system.html](http://www.cv.nrao.edu/~rfisher/Python/py_solar_system.html)

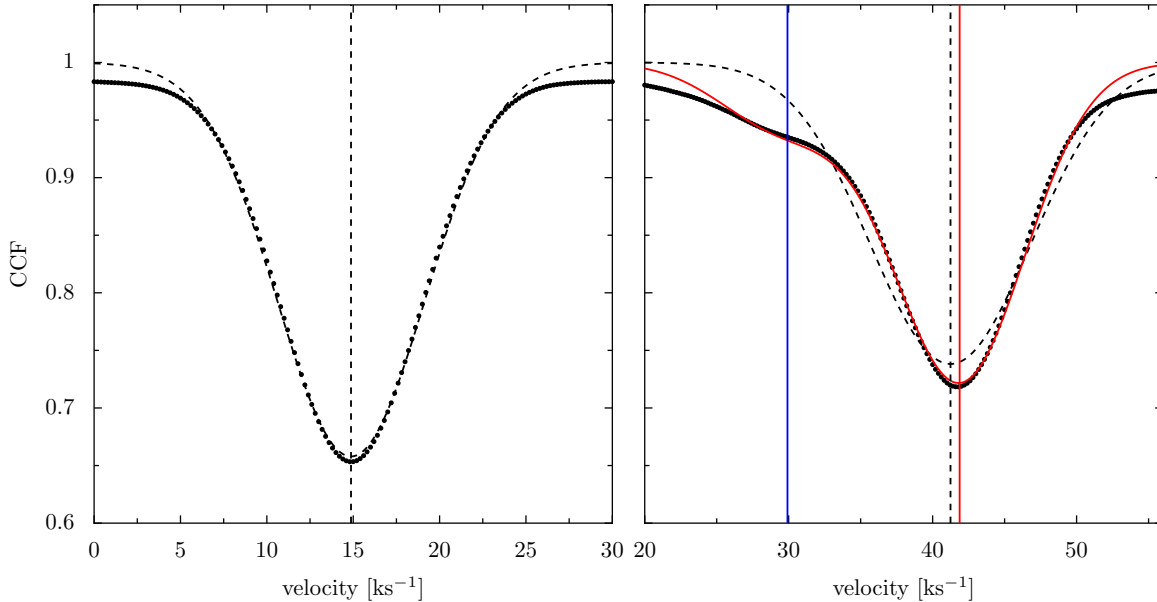


**Figure 6.** Left panel: peak of the CCF obtained from a FEROS spectrum of a solar type star and the G2 binary mask. The dotted line correspond to the CCF and the dashed line to the Gaussian fit. The vertical dashed line correspond to the mean of the Gaussian and the corresponding radial velocity value computed for this spectrum. Right panel: peak of the CCF obtained for a fainter star in the presence of significant scattered moonlight. The velocity position of the secondary peak in the CCF produced by the moon is marked by the vertical blue line. In this case the simple Gaussian fit does not deliver a reliable estimation of the radial velocity and a double gaussian fit is applied (red lines).

C and Fortran but can be called directly from Python. This velocity correction is computed by taking into account the integration time of the observation. The default procedure is to use the mid-time of the exposure to compute the barycentric velocity correction. However, if the spectrograph is equipped with an exposure meter, the time at which the detector has received half of the total flux is used as the input of the `jplephem` package.

### 2.6.2. Bisector Spans

Another useful parameter that can be extracted from the CCF is the bisector span (BS) which is a measure of the asymmetry of absorption lines. The absorption lines can be naturally asymmetric due to the Doppler broadening produced by convective motions in the surface of the star (macro turbulence). This effect produces the granulation of the stellar surface where the luminosity of the raising material is greater than the one of the material that is entering back the interior of the star. The observed spectrum corresponds to the disk integrated stellar intensity and the effect of the different intensities in the rising and receding material leads to the formation of asymmetric absorption lines. However, if the star has low levels of activity, the degree of asymmetry produced by convection is constant in time. Variations in the measured bisector spans can lead to variations in the measured radial velocities that can be associated with false positive scenarios. For example, eclipsing binary systems in which both peaks cannot be resolved in the CCF will produce this kind of behaviour in the single CCF peak. Similarly, stellar activity (spots and plages) leads to time correlated BS variations (see e.g. Desort et al., 2007; Boisse et al., 2011; Dumusque et al., 2014). In order to confirm the planetary nature of a TEP candidate, radial velocity and BS variations must be uncorrelated. CERES computes the BS from the CCF following Queloz et al. (2001b). The bisector is computed as the

mean velocity  $B(d)$  at the depth  $d$  between both sides of the CCF peak as

$$B(d) = \frac{v_l(d) + v_r(d)}{2}, \quad (7)$$

where, as shown in Figure 7,  $v_l$  correspond to the velocities located on the left side from the minimum of the CCF peak and  $v_r$  are the ones on the right side. Then, the mean bisector is computed at two depths ranges: from  $d = 0.1$  to  $d = 0.4$  and from  $d = 0.6$  to  $d = 0.85$  obtaining

$$\bar{B}_{0.1-0.4} = E[B(d)], \forall 0.1 < d < 0.4, \quad (8)$$

$$\bar{B}_{0.6-0.85} = E[B(d)], \forall 0.6 < d < 0.85. \quad (9)$$

Finally, the BS value is obtained from the difference of both quantities as

$$BS = \bar{B}_{0.1-0.4} - \bar{B}_{0.6-0.85}. \quad (10)$$

Figure 7 shows the parameters that are extracted from the CCF for computing the bisector span.

The errors in the BS measurements are estimated using a scaling relation that depends on the SNR in the region of the Mg triplet only as

$$\sigma_{BS} = \frac{a}{SN_{5130}} + b, \quad (11)$$

where  $a$  and  $b$  are coefficients determined from Monte Carlo simulations, with random noise added to high signal-to-noise ratio spectra for different spectral types, as was explained in § 2.6.1.

### 2.6.3. Rough stellar classification

CERES also includes a tool for fast estimation of stellar atmospheric parameters of the observed spectra. In order to estimate the stellar parameters ( $T_{\text{eff}}$ ,  $\log(g)$ ,  $[\text{Fe}/\text{H}]$ ,  $v \sin i$ ) we cross-correlate the observed spectrum against

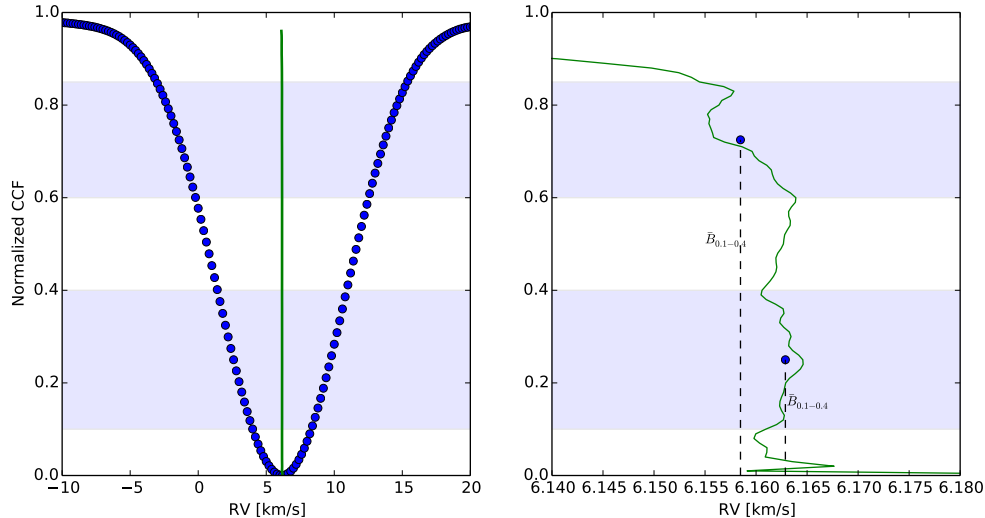


**Figure 7.** Left panel: the blue points correspond to the computed CCF, while the green line traces the bisector values at different depths. The coloured regions correspond to the two zones where the median bisectors are computed. Right panel: Zoom-in of the bisector values shown in the left panel, where the asymmetry of the CCF peak can be identified.

a grid of synthetic spectra of late-type stars from [Coelho et al. \(2005\)](#) convolved to the resolution of the spectrograph and a set of  $v \sin i$  values given by 0, 2.5, 5, 7.5, 10, 15, ..., 45, 50 km s<sup>-1</sup>. First, a set of atmospheric parameters is determined as a starting point by ignoring any rotation and searching for the model that produces the highest cross-correlation using only the Mg triplet region. We use a coarse grid of models for this initial step ( $\Delta T_{\text{eff}} = 1000 \text{ K}$ ,  $\Delta \log(g) = 1.0$ ,  $\Delta [\text{Fe}/\text{H}] = 1.0$ ). A new CCF between the observed spectrum and the model with the starting point parameters is then computed using a wider spectral region (4800 – 6200 Å). From this CCF we estimate radial velocity and  $v \sin i$  values using the peak position and width of the CCF, respectively. New  $T_{\text{eff}}$ ,  $\log(g)$ , and  $[\text{Fe}/\text{H}]$  values are then estimated by fixing  $v \sin i$  to the closest value present in our grid and searching for the set of parameters that gives the highest cross-correlation, and the new CCF is used to estimate new values of RV and  $v \sin i$ . This procedure is continued until convergence on stellar parameters is reached. For high signal-to-noise ratio spectra, uncertainties of this procedure are typically 200 K in  $T_{\text{eff}}$ , 0.3 dex in  $\log(g)$ , 0.2 dex in  $[\text{Fe}/\text{H}]$ , and 2 km s<sup>-1</sup> in  $v \sin i$ . These uncertainties were estimated from observations of stars with known stellar parameters from the literature. Results of our stellar parameter estimation procedure are obtained in  $\approx 2$  minutes using a standard laptop.

This tool is specially useful in the context of reconnaissance spectroscopy during the follow-up observations of transiting candidates, because it allows to make efficient use of the available observing time by quickly identifying some false positives or troublesome systems, such as fast rotators and giants, which are immediately dropped out from the target list. However, this module not expected to deliver high precision stellar parameters at publication level. For that purpose we have developed an alternative code (ZASPE [Brahm et al., 2016a](#)) that computes precise stellar atmospheric parameters with reliable errors, and uses as input the processed spectra obtained with

CERES.

### 3. CURRENTLY SUPPORTED INSTRUMENTS

Currently, CERES has been used to build fully automated reduction and analysis pipelines for thirteen echelle spectrographs, ranging from low-mid ( $R \approx 20000$ ) to high ( $R \approx 120000$ ) resolution spectrographs. A brief description of these instruments is given in the following paragraphs, while some specification can be found in [Table 1](#).

- CORALIE: This is a  $R=60,000$  echelle spectrograph installed at the 1.2m Euler/Swiss telescope at La Silla Observatory. It is fibre-fed from the telescope to a 2Kx2K CCD and includes also a second fibre that can be used to acquire a simultaneous spectrum of the sky or of a wavelength comparison source (ThAr lamp or Fabry-Perot etalon). It is placed in a fully controlled room where the temperature and vibrational conditions are stabilised. The current CERES pipeline is able to handle the ThAr and Fabry-Perot simultaneous calibration modes. The CERES pipeline developed for this instrument was briefly described in [Jordán et al. \(2014\)](#)
- FEROS ([Kaufer & Pasquini, 1998](#)): The Fibre-fed Extended Range Optical Spectrograph is installed at the 2.2m MPG telescope in La Silla Observatory and delivers a spectral resolution of  $R \approx 50000$  by using an image slicer. It has 39 orders which are registered by a 4Kx2K CCD and contains also a comparison fibre that can be used to obtain a simultaneous spectrum of the sky or a simultaneous ThAr lamp. It is placed in a separate room where the environmental conditions are monitored and stabilised.
- HARPS ([Queloz et al., 2001a](#)): The High Accuracy Radial velocity Planet Searcher is an echelle spectrograph installed at the 3.6m telescope in La

**Table 1**  
Properties of the instruments currently supported by CERES.

Name	Telescope	Type	Resolution $\times 1000$	Sampling px	Thermal stability	Vacuum vessel	CERES RV precision $\text{m s}^{-1}$
ARCES	APO 3.5m	Slit	30	2.8	No	No	Unknown
CAFE	CAHA 2.2m	Fibre	70	2.2	Yes	No	20
Coralie	Euler 1.2m	Fibre	60	3.5	Yes	Yes	7.8
FEROS	MPG 2.2m	Fibre	50	2.2	Yes (200 mK)	No	7.5
FIES	NOT 2.5m	Fibre	25, 46, 67	6.4, 3.4, 2.4	Tes (200 mK)	No	Unknown
FIDEOS	ESO 1.0m	Fibre	40	2.7	Yes	No	Unknown
HARPS	ESO 3.6m	Fibre	85, 120	4.3, 3.0	Yes (10 mK)	Yes	2.5
HIRES	Keck 10m	Slit	36, 48, 72	6.3, 4.7, 3.1	Yes	No	Unknown
ECHELLE	Du Pont 2.5m	Slit	30 – 50	2.3	No	No	500
ESPaDOnS	CFHT 3.6m	Fibre	80	3.5 – 2.1	Yes (100 mK)	Yes	Unknown
MIKE	Magellan 6.5m	Slit	20 – 80	7.1 – 1.8	No	No	Unknown
PFS	Magellan 6.5m	Slit	38 – 190	4.9 – 1.0	Yes	No	Unknown
PUCHEROS	PUC 0.5m	Fibre	20	2.8	No	No	200

Silla Observatory. It is one of the most ambient-stabilised fibre fed spectrographs in the world and is capable of detecting planets a few times more massive than the Earth. Its spectral resolution is  $R = 120000$  and it possesses 72 echelle orders which are registered by a 2 chip mosaic detector of total size 4Kx4K. It is housed in a vacuum vessel to avoid spectral drifts due to temperature and air pressure variations which produce instrumental variations  $< 1 \text{ m s}^{-1}$  along the night. It also possesses a second fibre that can be used to monitor the background sky or to obtain a simultaneous wavelength calibration.

- CAFE (Aceituno et al., 2013): The Calar Alto Fiber-fed Echelle spectrograph is installed in the 2.2m telescope at the Calar Alto Observatory in Spain. It is placed in a temperature and vibration controlled room but it does not count with a simultaneous calibration system. The resolution of this instrument is  $R \approx 70000$  and the complete optical spectrum is divided in 84 orders and registered in a 2Kx2K CCD. The radial velocity precision of the CERES pipeline for this instrument is  $\sigma_{RV} \approx 30 \text{ m s}^{-1}$ .
- ESPaDOnS (Donati, 2003): The Echelle SpectroPolarimetric Device for the Observation of Stars is installed at the 3.6m Canada-France-Hawaii Telescope in Manua Kea. It is a fiber-fed spectrograph that uses an image slicer to achieve a resolution of of 70000 and allows also to measure simultaneously circular and linear polarisations. The CERES pipeline can process ESPaDOnS data obtained with the three different observing modes (star, star + sky, polarimetry).
- PUCHEROS (Vanzi et al., 2012): This instrument is a  $R = 20000$  fibre fed echelle spectrograph built by the Centro de Astroingenieria at PUC/Chile and installed at the 0.5m telescope of the Observatorio UC near Santiago. It is not placed in a controlled room and does not count with a simultaneous wavelength calibration system. The CERES pipeline is the reduction system for this instrument and is installed at the observatory. The small aperture of the telescope translates in that most of the

observations have low SNR for which the optimal extraction of the CERES pipeline plays a fundamental role in delivering good quality data.

- FIES (Telting et al., 2014): the Fiber-fed Echelle Spectrograph is installed at the 2.5m Nordic Optical Telescope. It has three different fibres which deliver resolutions of 25000, 46000 and 67000, respectively. It also has a fourth fibre that can be used to obtain to perform a simultaneous wavelength calibration. The current version of the pipeline can process only data obtained with the low-res and high-res fibres without simultaneous calibration.
- FIDEOS (Tala et al., 2014): The Fibre Dual Echelle Optical Spectrograph was recently installed on the 1m telescope at La Silla Observatory. Its object fibre has a image slicer which deliver a resolution of  $R = 40000$ . It has also a comparison fibre that can be used to perform simultaneous wavelength calibration. Given that the instrument is still in the commissioning stage, the current CERES pipeline will probably be updated.
- DuPont/Echelle: This instrument is an echelle spectrograph mounted on the 2.5m DuPont telescope in Las Campanas Observatory. This spectrograph is very unstable and the flexures of the telescope produce that the vertical and horizontal positions of the orders change with the position of the telescope. However the pipeline is able to retrace the orders and deal with these stability related issues.
- MIKE (Bernstein et al., 2003): The Magellan Inamori Kyocera Echelle spectrograph is mounted on the 6.5m Clay telescope at Las Campanas Observatory. The spectra is separated into two arms and both portions are registered in different CCDs. Currently the CERES pipeline can only process the red arm (4900 Å-9500 Å) with the 1'' slit that delivers a resolution of  $R = 65000$ . This instrument is also mounted directly on the telescope which strongly affects the achievable RV precision.
- PFS (Crane et al., 2006): The Carnegie Planet Finder Spectrograph is also mounted on the Clay

telescope but this instrument uses the I<sub>2</sub> cell technique for achieving precise radial velocity measurements. The official pipeline developed and managed by the PFS team delivers a radial velocity precision of  $\sigma_{RV} \approx 2 \text{ m s}^{-1}$  for bright stars. The CERES pipeline does not handle data with I<sub>2</sub> cell and for the moment it only relies on the wavelength calibration provided by a ThAr lamp.

- ARCES (Wang et al., 2003): The ARC Echelle Spectrograph is mounted on the 3.5m telescope at the Apache Point Observatory in New Mexico, USA, and has a spectral resolution of  $R = 31000$ .
- HIRES (Vogt et al., 1994): The High Resolution Echelle Spectrometer is mounted on Keck in Hawaii. The complete optical spectrum is registered in 3 CCDs but currently, the CERES pipeline can only reduce data of the green chip (5000 Å-6000 Å) and does not compute radial velocities with the I<sub>2</sub>-cell technique.

#### 4. PERFORMANCE AND INTERESTING RESULTS

The computational routines and recipes developed for CERES were designed with the main goal of performing spectroscopic follow-up observations of transiting planetary candidates from the HATSouth survey (Bakos et al., 2009). Therefore, the tools we have presented were optimised for obtaining homogeneous results from low to moderate signal to noise ratio data ( $\text{SNR} \sim 20\text{-}50$ ), including radial velocities precise enough to measure variations produced by massive planetary companions ( $5\text{-}100 \text{ m s}^{-1}$ ) and atmospheric parameters with enough precision to have an informed guess about the physical parameters of the observed stars.

We have been monitoring the radial velocity precision of our pipelines for each spectrograph by observing radial velocity standard stars. Figure 8 shows the radial velocity measurements for these standard stars in the case of four different instruments, and Table 2 lists the individual dispersion values of the measured radial velocities for each spectrograph. Figure 8 shows that while the long term precision achieved by fibre-fed and stabilised instruments is below  $10 \text{ m s}^{-1}$ , the precision obtained by the non stabilised spectrograph is of the order of  $400 \text{ m s}^{-1}$ , which is not enough for detecting variations produced by planetary mass companions, but is sufficient for quickly identifying stellar or brown dwarf companions, which are common false positive systems in dedicated ground-based surveys of transiting planets. Given that the CERES pipelines are also capable of estimating stellar atmospheric parameters and computing bisector spans, the spectra obtained with the DuPont echelle can be used to efficiently identify other kind of false positives, namely, giant stars, fast rotators and blended eclipsing binaries. The automatization of the reduction steps make of the CERES pipeline for the duPont echelle an optimal system for performing the reconnaissance spectroscopy steps of the follow-up observations of transiting surveys, specially because there is no dedicated reduction system for this instrument. The CERES pipeline for the DuPont/echelle has been only tested for 2 slit configurations, namely  $1'' \times 4''$  and  $0.75'' \times 4''$ , which correspond

**Table 2**  
Properties of the radial velocity standard stars.

ID	Spectral type	$\sigma_{RV}^{\text{coralie}}$ $\text{m s}^{-1}$	$\sigma_{RV}^{\text{feros}}$ $\text{m s}^{-1}$	$\sigma_{RV}^{\text{harps}}$ $\text{m s}^{-1}$
HD72673	G9V	8.0	7.3	2.6
HD157347	G3V	7.3	7.9	2.3
HD32147	K3V	8.5	8.0	–

to spectral resolutions of  $R \approx 40000$  and  $R \approx 50000$ , respectively.

The results obtained with the CERES pipelines for stabilised fibre-fed instruments (CORALIE, FEROS and HARPS), are precise enough for allowing the detection of planetary mass companions. The accuracy obtained for the HARPS spectrograph is slightly worse than the one obtained by the official Data Reduction Software, which is expected given the large amount of effort and numerous upgrades that have been applied on the official dedicated pipeline. The radial velocity precision achieved in the case of the CORALIE and FEROS pipelines is of  $\approx 7 \text{ m/s}$ . This precision is similar to the one obtained by the official (non-public) CORALIE pipeline, but is significantly better than the  $\approx 30 \text{ m s}^{-1}$  precision achieved by the dedicated FEROS pipeline installed at the telescope. In addition to the high precision achieved in the high signal to noise ratio regime, the FEROS pipeline based on CERES routines can handle data with low signal to noise ratio ( $\text{SNR} < 30$ ) obtaining radial velocity uncertainties governed by Poisson errors, as opposed to the official pipeline, whose velocity errors become dominated by systematics that are not removed in the reduction steps. A strong proof of the capabilities of our CERES pipeline for FEROS is the discovery of HATS-20b (Bhatti et al., 2016), a Saturn-mass transiting planet around a  $V = 14$  solar type star, that produces a  $K = 40 \text{ m s}^{-1}$  keplerian signal that was identified using 10 FEROS exposures of 1800s. An important peculiarity of our CERES pipeline for FEROS is that it does not process all the echelle orders because we have found that the precision of the wavelength solution significantly worsens if all of them are included in the fit. Therefore, our final FEROS output has 25 echelle orders covering only from 3800 Å to 6800 Å.

These CERES pipelines developed for FEROS and CORALIE have been fundamental for confirming the planetary nature of most of the discovered transiting planets from the HATSouth survey (see e.g. Brahm et al., 2015; Mancini et al., 2015; Rabus et al., 2016; Ciceri et al., 2015; Brahm et al., 2016c), and equally important to reject a much larger fraction of false positives.

Due to the high precision and homogeneity of the obtained results, the CERES pipelines, in particular the ones for CORALIE and FEROS have been already used in different studies with different scientific goals, which we briefly mention here as a demonstration of their scope:

- Kepler K2 planets: Espinoza et al. (2016) presented the discovery of a dense Neptune mass planet using data from the CORALIE and HARPS spectrographs. Brahm et al. (2016b) presented the discovery of two hot Jupiters, firstly identified as transiting candidates from K2 photometry, and which

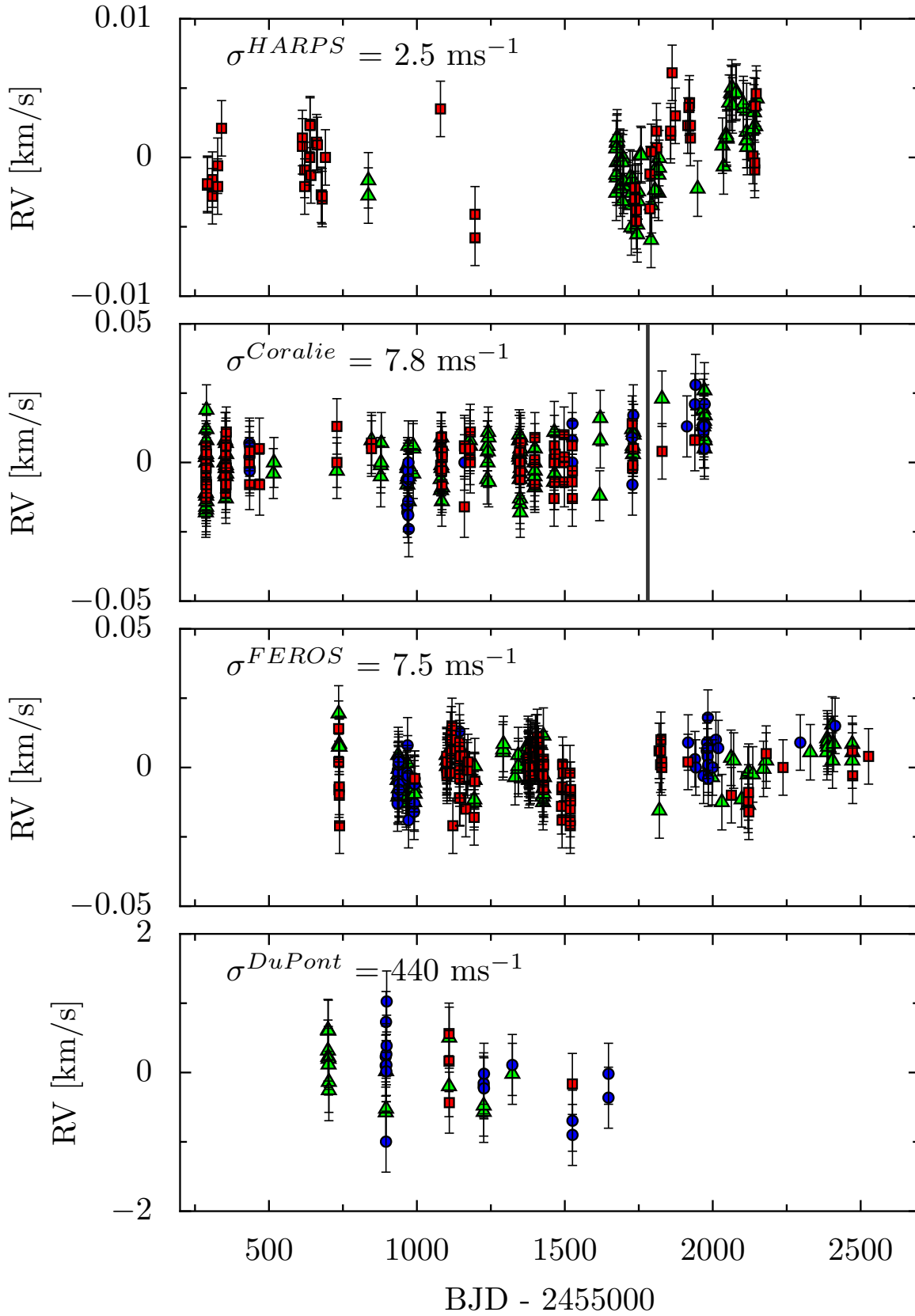


**Figure 8.** Radial velocity measurements for 3 radial velocity standard stars (squares: HD2673, triangles: HD157347, circles: HD32147) obtained with four different instruments (from top to bottom: HARPS, CORALIE, FEROS, DuPont) using the CERES pipelines. The vertical line in the second panel corresponds to the date where the instrument was upgraded, which produced a  $\sim 20 \text{ ms}^{-1}$  offset in the radial velocities.

planetary nature was confirmed via precision radial velocities from the CORALIE, FEROS and HARPS spectrographs. [Crossfield et al. \(2016\)](#) presented the validation of 104 planets from K2, for which FEROS observations reduced with CERES were used.

- Radial velocity planets: Using HARPS and CORALIE data, [Jenkins et al. \(2016\)](#) announced the discovery of eight new planetary systems containing giant planets. [Wittenmyer et al. \(2016\)](#) and [Jones et al. \(2016\)](#) presented the discovery of five new systems conformed of giant planets orbiting giant stars by using data from the FEROS spectrograph among others.
- Studies on already discovered extrasolar plates: [Ciceri et al. \(2016\)](#) and [Mancini et al. \(2016\)](#) updated the physical parameters of the WASP-45b, WASP-46 and WASP-98 planetary systems by obtaining new spectroscopic and photometric observations of these transiting hot Jupiters. The spectroscopic data was obtained with FEROS.
- Detached eclipsing binaries: [Helminiak et al. \(2014\)](#) and [Coronado et al. \(2015\)](#) presented the orbital and physical parameters of two new detached eclipsing systems that were identified from ASSAS photometry, and then followed-up with the FEROS, CORALIE, HARPS and PUCHEROS spectrographs.
- Search of supernova progenitors: Combining data from RAVE, GALEX, HST and FEROS, [Parsons et al. \(2015\)](#) reported the discovery the first pre-supernova X-ray binary.
- Identification of members of young associations: [Elliott et al. \(2016\)](#) presented the discovery of 84 low mass stars that are linked to young associations. A fraction of those new members were confirmed using radial velocities from FEROS reduced with CERES.
- Spectroscopic follow-up of Novae: [Izzo et al. \(2015\)](#) presented the first detection of lithium produced in the optical spectra of a Nova using early CERES spectra from FEROS and PUCHEROS.

## 5. CONCLUSIONS

We have presented CERES, a set of routines that allow the development of robust and fully automated pipelines for the reduction, processing and analysis of echelle spectra. We have constructed pipelines for thirteen different instruments with quite different specifications, reaching results that are almost as good or better than those of dedicated pipelines when available. In this regard, the CERES pipeline for the FEROS spectrograph stands out due to the high RV precision that can be achieved in the high signal-to-noise ratio regimen ( $\sigma_{RV}=7.5 \text{ ms}^{-1}$ ), and also for its good behaviour for low signal-to-noise ratio data, which has allowed the discovery of several extrasolar planets orbiting stars even fainter than  $V = 14$ . Moreover, we have developed reduction pipelines for instruments that do not have any dedicated pipeline, like

the one for the DuPont spectrograph, for which we can achieve an RV precision of  $\sigma_{RV}=400 \text{ ms}^{-1}$  and complete automatization despite the lack of stability of the instrument. The recipes for these thirteen instruments can be used as guide for constructing pipelines for other instruments. In addition to reduced spectra, radial velocities and bisector spans, the CERES pipelines estimate rough and fast atmospheric parameters which are useful for quick target vetting at the telescope.

There are several limitations of CERES that are being considered for future upgrades. For example, our extraction algorithms do not perform a previous rectification of the curvature of the echelle orders. The correction for the curvature can increase the resolution of the extracted spectrum, but it could introduce complications for the optimal extraction algorithm because it will require an interpolation between pixels. In addition, given that the principal applications of CERES have been focused on fibre-fed spectrograph, it does not contain a routine to correct for sky contamination, which can be useful in the case of slit spectrographs. Finally, an important upgrade for CERES will consist in developing automated routines for the computation of precise radial velocities using the iodine cell technique.

The full CERES code, along with the pipelines for the instruments described in Section 3 have been made publicly available<sup>7</sup>.

We thank Gaspar Bakos and Joel Hartman for many useful discussions and strong encouragement to develop and improve the code presented in this work. A.J. thanks Didier Queloz with whom he had many fruitful discussions regarding radial velocity measurements in the early development stages of CERES. R.B. and N.E. are supported by CONICYT-PCHA/Doctorado Nacional. A.J. acknowledges support from FONDECYT project 1130857 and from BASAL CATA PFB-06. R.B., N.E. and A.J. acknowledge support from the Ministry for the Economy, Development, and Tourism Programa Iniciativa Científica Milenio through grant IC 120009, awarded to the Millennium Institute of Astrophysics (MAS). This paper made use of the SIMBAD database (operated at CDS, Strasbourg, France), NASA's Astrophysics Data System Bibliographic Services, and data products from the Two Micron All Sky Survey (2MASS) and the APASS database and the Digitized Sky Survey.

## REFERENCES

- Aceituno, J., Sánchez, S. F., Grupp, F., et al. 2013, *A&A*, 552, A31
- Bakos, G., Afonso, C., Henning, T., et al. 2009, in *IAU Symposium*, Vol. 253, IAU Symposium, ed. F. Pont, D. Sasselov, & M. J. Holman, 354–357
- Ballester, P. 1992, in *European Southern Observatory Conference and Workshop Proceedings*, Vol. 41, European Southern Observatory Conference and Workshop Proceedings, ed. P. J. Grosbøl & R. C. E. de Ruijscher, 177
- Banase, K., Crane, P., Grosbol, P., et al. 1983, *The Messenger*, 31, 26
- Baranne, A., Queloz, D., Mayor, M., et al. 1996, *A&AS*, 119, 373
- Bernstein, R., Shectman, S. A., Gunnels, S. M., Mochnacki, S., & Athey, A. E. 2003, in *Proc. SPIE*, Vol. 4841, *Instrument Design and Performance for Optical/Infrared Ground-based Telescopes*, ed. M. Iye & A. F. M. Moorwood, 1694–1704

<sup>7</sup> <https://github.com/rabrahm/ceres>

- Bhatti, W., Bakos, G. Á., Hartman, J. D., et al. 2016, ArXiv e-prints, 1607.00322
- Bochanski, J. J., Hennawi, J. F., Simcoe, R. A., et al. 2009, *PASP*, 121, 1409
- Boisse, I., Bouchy, F., Hébrard, G., et al. 2011, *A&A*, 528, A4
- Brahm, R., Jordan, A., Hartman, J., & Bakos, G. 2016a, ArXiv e-prints, 1607.05792
- Brahm, R., Jordán, A., Hartman, J. D., et al. 2015, *AJ*, 150, 33
- Brahm, R., Jones, M., Espinoza, N., et al. 2016b, ArXiv e-prints, 1603.01721
- Brahm, R., Jordán, A., Bakos, G. Á., et al. 2016c, *AJ*, 151, 89
- Cabrera, J., Bruntt, H., Ollivier, M., et al. 2010, *A&A*, 522, A110
- Ciceri, S., Mancini, L., Henning, T., et al. 2015, ArXiv e-prints, 1511.06305
- Ciceri, S., Mancini, L., Southworth, J., et al. 2016, *MNRAS*, 456, 990
- Coelho, P., Barbuy, B., Meléndez, J., Schiavon, R. P., & Castilho, B. V. 2005, *A&A*, 443, 735
- Coronado, J., Helminiak, K. G., Vanzì, L., et al. 2015, *MNRAS*, 448, 1937
- Crane, J. D., Shtetman, S. A., & Butler, R. P. 2006, in *Proc. SPIE*, Vol. 6269, Society of Photo-Optical Instrumentation Engineers (SPIE) Conference Series, 626931
- Crossfield, I. J. M., Ciardi, D. R., Petigura, E. A., et al. 2016, ArXiv e-prints, 1607.05263
- Dekker, H., D’Odorico, S., Kaufer, A., Delabre, B., & Kotzłowski, H. 2000, in *Proc. SPIE*, Vol. 4008, Optical and IR Telescope Instrumentation and Detectors, ed. M. Iye & A. F. Moorwood, 534–545
- Desort, M., Lagrange, A.-M., Galland, F., Udry, S., & Mayor, M. 2007, *A&A*, 473, 983
- Donati, J.-F. 2003, in *Astronomical Society of the Pacific Conference Series*, Vol. 307, Solar Polarization, ed. J. Trujillo-Bueno & J. Sanchez Almeida, 41
- Dumusque, X., Boisse, I., & Santos, N. C. 2014, *ApJ*, 796, 132
- Elliott, P., Bayo, A., Melo, C. H. F., et al. 2016, *A&A*, 590, A13
- Espinoza, N., Brahm, R., Jordán, A., et al. 2016, ArXiv e-prints, 1601.07608
- Giguere, M. J., Fischer, D. A., Payne, M. J., et al. 2015, *ApJ*, 799, 89
- Griffin, R. F. 1967, *ApJ*, 148, 465
- Halverson, S., Mahadevan, S., Ramsey, L., et al. 2014, *PASP*, 126, 445
- Halverson, S., Terrien, R., Mahadevan, S., et al. 2016, ArXiv e-prints, 1607.05634
- Helminiak, K. G., Brahm, R., Ratajczak, M., et al. 2014, *A&A*, 567, A64
- Horne, K. 1986, *PASP*, 98, 609
- Izzo, L., Della Valle, M., Mason, E., et al. 2015, *ApJ*, 808, L14
- Jenkins, J. S., Jones, H. R. A., Tuomi, M., et al. 2016, ArXiv e-prints, 1603.09391
- Jones, M. I., Jenkins, J. S., Brahm, R., et al. 2016, *A&A*, 590, A38
- Jordán, A., Brahm, R., Bakos, G. Á., et al. 2014, *AJ*, 148, 29
- Kaufer, A., & Pasquini, L. 1998, in *Society of Photo-Optical Instrumentation Engineers (SPIE) Conference Series*, Vol. 3355, Optical Astronomical Instrumentation, ed. S. D’Odorico, 844–854
- Li, C.-H., Benedict, A. J., Fendel, P., et al. 2008, *Nature*, 452, 610
- Mancini, L., Giordano, M., Mollière, P., et al. 2016, *MNRAS*
- Mancini, L., Hartman, J. D., Penev, K., et al. 2015, *A&A*, 580, A63
- Marsh, T. R. 1989, *PASP*, 101, 1032
- Mayor, M., & Queloz, D. 1995, *Nature*, 378, 355
- Mayor, M., Pepe, F., Queloz, D., et al. 2003, *The Messenger*, 114, 20
- Mills, D., Webb, J., & Clayton, M. 2003, *Starlink User Note*, 152
- Mink, D. J. 2011, in *Astronomical Society of the Pacific Conference Series*, Vol. 442, *Astronomical Data Analysis Software and Systems XX*, ed. I. N. Evans, A. Accomazzi, D. J. Mink, & A. H. Rots, 305
- Noguchi, K., Aoki, W., Kawanomoto, S., et al. 2002, *PASJ*, 54, 855
- Parsons, S. G., Schreiber, M. R., Gänsicke, B. T., et al. 2015, *MNRAS*, 452, 1754
- Queloz, D. 1995, in *IAU Symposium*, Vol. 167, *New Developments in Array Technology and Applications*, ed. A. G. D. Philip, K. Janes, & A. R. Uppgren, 221
- Queloz, D., Mayor, M., Udry, S., et al. 2001a, *The Messenger*, 105, 1
- Queloz, D., Henry, G. W., Sivan, J. P., et al. 2001b, *A&A*, 379, 279
- Rabus, M., Jordán, A., Hartman, J. D., et al. 2016, ArXiv e-prints, 1603.02894
- Reiners, A., Banyal, R. K., & Ulbrich, R. G. 2014, *A&A*, 569, A77
- Sarmiento, L. F., Reiners, A., Seemann, U., et al. 2014, in *Proc. SPIE*, Vol. 9147, *Ground-based and Airborne Instrumentation for Astronomy V*, 914754
- Sosnowska, D., Lovis, C., Figueira, P., et al. 2015, in *Astronomical Society of the Pacific Conference Series*, Vol. 495, *Astronomical Data Analysis Software and Systems XXIV (ADASS XXIV)*, ed. A. R. Taylor & E. Rosolowsky, 285
- Stürmer, J., Seifahrt, A., Schwab, C., & Bean, J. L. 2016, ArXiv e-prints, 1607.05172
- Suzuki, N., Tytler, D., Kirkman, D., O’Meara, J. M., & Lubin, D. 2003, *PASP*, 115, 1050
- Tala, M., Berdja, A., Jones, M., et al. 2014, in *Proc. SPIE*, Vol. 9147, *Ground-based and Airborne Instrumentation for Astronomy V*, 914789
- Telting, J. H., Avila, G., Buchhave, L., et al. 2014, *Astronomische Nachrichten*, 335, 41
- Vanzì, L., Chacon, J., Helminiak, K. G., et al. 2012, *MNRAS*, 424, 2770
- Vogt, S. S., Allen, S. L., Bigelow, B. C., et al. 1994, in *Proc. SPIE*, Vol. 2198, *Instrumentation in Astronomy VIII*, ed. D. L. Crawford & E. R. Craine, 362
- Wang, S.-i., Hildebrand, R. H., Hobbs, L. M., et al. 2003, in *Proc. SPIE*, Vol. 4841, *Instrument Design and Performance for Optical/Infrared Ground-based Telescopes*, ed. M. Iye & A. F. M. Moorwood, 1145–1156
- Wittenmyer, R. A., Johnson, J. A., Butler, R. P., et al. 2016, *ApJ*, 818, 35